Faraday Discussions

Cite this: *Faraday Discuss.*, 2019, **216**, 162

PAPER

View Article Online
View Journal | View Issue

Systematic control of the rate of singlet fission within 6,13-diphenylpentacene aggregates with PbS quantum dot templates†

Chen Wang, [a] Mohamad S. Kodaimati,[b] Shichen Lian[b] and Emily A. Weiss *[b]

Received 24th October 2018, Accepted 20th December 2018
DOI: 10.1039/c8fd00157j

Lead chalcogenide quantum dots (QDs) are promising acceptors for photovoltaic devices that harness the singlet fission (SF) mechanism. The rate of singlet fission of polyacenes in the presence of QDs is a critical parameter in determining the performance of such devices. The present study demonstrates that the rates of SF in a pentacene derivative, 6,13-diphenylanthracene (DPP), are modulated by forming coaggregates with PbS QDs in aqueous dispersions. PbS QDs generally accelerate SF within DPP aggregates, and the extent of acceleration depends on the size of the QD. The average rate of SF increases from 0.074 ps^{-1} for DPP-only aggregates to 0.37 ps^{-1} within DPP-D co-aggregates for QDs with radius 2.2 nm, whereas co-aggregation with the smallest (r = 1.6 nm) and largest (r = 2.7 nm) QDs we tried only slightly change the SF rate. The rate variation is associated with (i) the density of surface ligands, which is influenced by the faceting of the PbS surface, and (ii) the local dielectric constant for DPP. To accelerate SF, the ligands should be dense enough to provide sufficient affinity for DPP aggregates and effectively perturb the perpendicular alignment of DPP monomers within aggregates to increase the intermolecular coupling that promotes SF, but should not be too dense so as to form a low dielectric environment that disfavors SF. The study suggests that it is critical to consider the influence of the microenvironment of the QD surface on photophysical processes when fabricating QD/organic hybrid devices.

Introduction

The paper describes the control of the rate of singlet fission (SF) within aggregates of 5,13-diphenylpentacene (DPP) adsorbed to the surfaces of colloidal PbS

[a]*Department of Chemistry and Biochemistry, City University of New York, Queens College, 65-30 Kissena Blvd., Flushing, NY, 11367, USA*

[b]*Department of Chemistry, Northwestern University, 2145 Sheridan Rd., Evanston, IL 60208-3113, USA. E-mail: e-weiss@northwestern.edu*

† Electronic supplementary information (ESI) available. See DOI: 10.1039/c8fd00157j

quantum dots (QDs) that are also capped with poly(ethylene glycol)thiolate (PEGT), in water. Singlet fission is a photophysical process that produces two triplet excited states from one singlet excited state. The SF mechanism is a possible route to increasing the efficiency of organic photovoltaic devices beyond the Shockley–Queisser limit.[1–4] Polyacene materials are promising candidates for devices that employ the singlet fission mechanism,[5,6] and the dynamics of singlet fission of polyacenes and their derivatives have been studied in detail, both in isolated aggregates[7–19] and aggregates adsorbed to gold nanoparticles.[20] The rate of the SF process is a crucial parameter for designing photovoltaic devices utilizing this mechanism; this rate should be maximized, not only to ensure the efficient generation of triplet excitons, but also to outcompete direct charge separation from the singlet excited state.[21,22] It is known that the alignment of SF chromophores within the SF material determines their intermolecular coupling, which plays a crucial role in determining the rate of formation of the SF precursor state, a correlated triplet pair $^1(T_1T_1)$, and in determining the rate of dissociation of the two triplet excitons.[5,21,23–26] The dielectric environment of the organic aggregate can also affect the SF rate,[27] because SF is mediated by a charge transfer intermediate.[28,29] Systematic control of the SF rate on the surface of a particle like a colloidal QD, where the properties of the QD scaffold are controllable through both size and surface chemistry, provides insight into the structural parameters that influence SF, and the efficiency of subsequent transfer of triplet excitons[30,31] or photoelectrons[32,33] to a QD, which could serve as a complementary active material in a solar cell.

This work demonstrates that the surface of a QD and it solubilizing ligands serve as a template for the assembly of DPP, as it has for other organic dye molecules.[34–38] Here, we show that this scaffolding effect influences the dynamics of singlet fission within adsorbed DPP aggregates, to a degree that depends on the size of the QD. We prepared PbS QD/DPP co-aggregates, with QDs of six different radii, in aqueous solution, and characterized the sizes and shapes of the co-aggregates with dynamic light scattering (DLS), and transmission electron microscopy (TEM). We evaluated the rate of the SF process of DPP in these co-aggregates using transient absorption (TA) spectroscopy, and found that, for most sizes of QDs, co-aggregation of DPP with QDs accelerates singlet fission. In particular, when DPP is co-aggregated with QDs with a radius of 2.2 nm, the singlet fission rate is 5-fold faster than that in the pure DPP aggregate, but co-aggregation with the very large (r = 2.7 nm) and very small (r = 1.6 nm) QDs does not substantially affect the SF rate.

Experimental

Preparation of poly(ethylene glycol)thiolate-(PEGT) capped PbS quantum dots

We synthesized PbS QDs capped with oleate using a protocol adapted from Hines *et al.*[39] (see the ESI†). To prepare water-soluble PbS QDs, we exchanged the oleate ligands for PEGT (MW = 1000, Sigma-Aldrich). We dissolved oleate-capped QDs in 0.3 ml $CHCl_3$ to form a 50 μM solution. PEGT ligands were dissolved in methanol in a concentration of 100 mg ml^{-1}. Different amounts of PEGT were added to the QD dispersion for different radii of QDs to ensure minimum but sufficient amounts of PEGT in the ligand exchange process; specifically: for r = 1.6 nm, 250 eq.; r = 1.8 nm, 300 eq.; r = 2.0 nm, 400 eq.; r = 2.2 nm, 500 eq.; r =

2.4 nm, 600 eq.; $r = 2.7$ nm, 800 eq. per QD. We allowed the QD/PEGT mixtures to react for at least 10 h, and precipitated the QDs by adding 6 ml of a mixture of $CHCl_3$/ethanol/hexanes (1 : 1 : 10, v/v/v) and centrifuging at 8000 rpm for 5 min. We washed the pellet with the same solvent mixture and recollected the QDs by centrifuging to remove extra PEGT ligands. The wash/centrifugation cycle was repeated twice. The final pellet was dried under N_2 flow, and redispersed in 3 ml of water. The sample solution was filtered using syringe filters with a pore size of $\leq$0.22 μm, diluted to 1 μM, and purged with $Ar_{(g)}$ for 10 min before being moved into an N_2-filled box.

Preparation of QD–DPP assemblies

We prepared the QD–DPP assemblies in an N_2-filled box. We dissolved DPP in acetonitrile to form a nearly saturated solution ($\sim$0.5 mM), and added 0.2 ml of DPP solution to 1.8 ml of 1 μM QDs $_{(aq)}$ while stirring vigorously. The samples were sonicated for 1 hour before use.

Transient absorption spectroscopy

Details of the TA setup can be found elsewhere.[40] Briefly, fs-TA experiments were conducted using a commercial system (Ultrafast Systems LLC, Helios) powered by a Ti:sapphire amplifier (Spectra-Physics, Solstice). The 800 nm, 2.5 mJ, 100 fs pulse generated by the amplifier was split into two to generate pump and probe beams. The pump beam was directed through an optical parametric amplifier (Light Conversion, TOPAS-C) with sum-frequency generation to produce pump pulses at wavelengths of 600 and 970 nm. The probe beam containing a small portion of the amplifier output was directed through a 3 mm thick sapphire window to generate a white light continuum probe in the spectral region. The pump and the probe were focused and overlapped at the sample, which was contained in a 2 mm quartz cuvette. During data collection, all samples were stirred continuously. The instrument response function (IRF) of the TA setup was determined by measuring the full-width-at-half-maximum of the optical Kerr effect response of the acetonitrile/water (10%, v/v) solution in the same quartz cuvette. The IRF was 200 fs for the TA experiment.

Results and discussion

Fig. 1A shows that mixing DPP with PbS QDs does not affect the electronic transitions of the QDs. The first excitonic band of the QDs, at 1220 nm, does not shift or broaden after mixing with DPP. The enhancement of the absorption at wavelengths below 500 nm is primarily due to the absorption of DPP but also has contribution from scattering of the aggregates discussed below.

Fig. 1B shows the spectra of disaggregated DPP ("DPP Mon"), aggregated DPP with no QDs ("DPP Agg"), and DPP in mixtures with QDs ($r = 2.2$ nm) ("QD + DPP"), after the spectra of the QDs have been subtracted (see the ESI†). The formation of aggregates of DPP results in a 530 cm^{-1} bathochromic shift of its absorption spectrum. The shift is primarily due to dispersive interactions of the excitons in DPP aggregates, as reported for other molecular aggregate systems.[41] The shift within DPP-only aggregates is not however attributable to J-aggregation because: (1) there is no significant change in the vibronic progression upon the

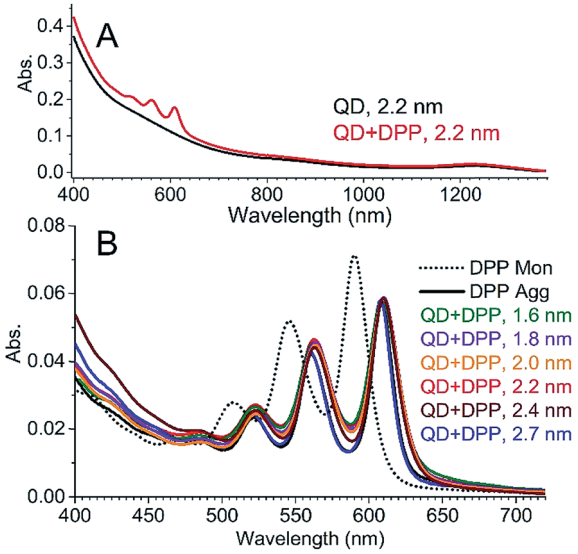

Fig. 1 (A) Ground state absorption spectra of PbS QDs with $r = 2.2$ nm and their assemblies with DPP in 10% (v/v) acetonitrile/water. (B) Absorption spectra of the DPP monomer in acetonitrile, DPP aggregates in water, and DPP in the presence of PbS QDs of six different radii. The spectra of DPP within the "QD–DPP" samples were obtained by subtracting the absorption spectra of the PbS QDs from the co-aggregate spectra, see the ESI.†

formation of the aggregate – that is, in the aggregate spectrum, the relative intensities of the (0–0) (~610 nm) and (0–1) (~560 nm) transitions are very similar to those of the ~590 and ~550 nm peaks in the monomer spectrum[42] – and (2) crystallography data of DPP samples with similar spectral features show that adjacent DPP molecules are aligned perpendicularly, which prevents exciton coupling between their transition dipoles.[21]

There are subtle differences among the absorption spectra of the QD–DPP samples depending on the radius of the QDs. The spectrum for the sample with the largest QDs ($r = 2.7$ nm) overlays with that of the DPP aggregate without QDs. For QDs with radii of 1.6 nm, 1.8 nm, 2.0 nm, and 2.2 nm, in the QD–DPP co-aggregate spectra there is a 120-to-160 cm^{-1} broadening of the 0–0 vibronic band, and a ~100 cm^{-1} bathochromic shift of the 0–1 vibronic band, compared to that of the pure DPP aggregate. The spectrum of the mixture of DPP with $r =$ 2.4 nm QDs appears to be intermediate between those of the undisturbed DPP aggregate and the QD–DPP co-aggregate.

These perturbations of the DPP aggregate spectra by the QDs is most likely due to interaction between DPP and the PEGT ligands of the QDs, which can disturb the perpendicular packing of DPP molecules, and thereby induce weak exciton coupling within the DPP aggregates. Such coupling would cause a bathochromic shift and heterogeneous broadening of the absorption peaks. The $r = 2.7$ nm QDs do not appear to cause such a perturbation.

We supported the aforementioned hypothesis with transmission electron micrographs (TEM) of the QDs and the QD–DPP mixtures (Fig. 2) with four sizes of

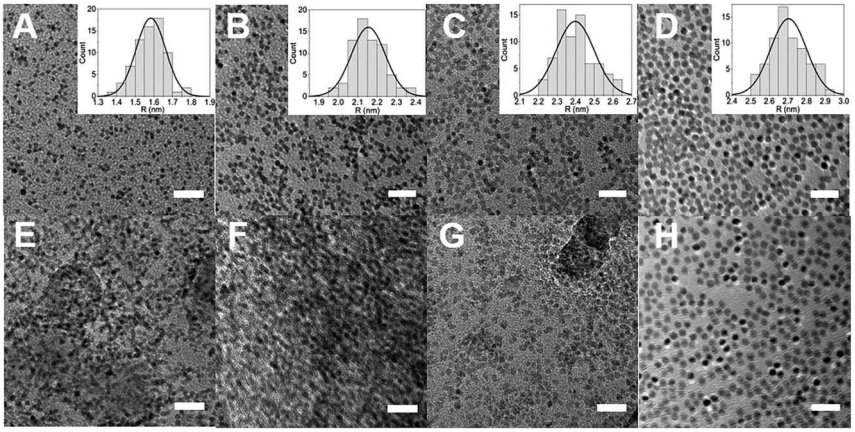

Fig. 2 TEM images of QDs of four different radii (A–D) and their assemblies with DPP (E–H). The radii of PbS QDs, determined by fitting the sizing histograms for 70 particles with Gaussian functions (insets), are 1.6 ± 0.2 nm (A and E), 2.2 ± 0.2 nm (B and F), 2.4 ± 0.2 nm (C and G) and 2.7 ± 0.2 nm (D and H). Scale bars in all images indicate 20 nm.

QDs. When there is no DPP present, the QDs are well-dispersed, or only form small clusters, on the TEM grids (Fig. 2A–D). When the 1.6 nm, 2.2 nm, and 2.4 nm QDs are mixed with DPP in solution and deposited on the TEM grid, however, we observe large QD agglomerates with blurry profiles for individual nanoparticles (Fig. 2E–G). Although we cannot capture images of the DPP assemblies because of the low contrast of the organic material in comparison with the QDs, these images indicate the formation of co-aggregated DPP and QDs, which decreases the contrast and focus of the image. The sizes of the QD–DPP aggregates are irregular, varying from 30 to 80 nm in diameter, which agrees with the results of DLS measurements (see the ESI†). The only exception is the largest QDs ($r = 2.7$ nm), which do not form co-aggregates with DPP (Fig. 2H). Given that the absorption spectrum of the QD (2.7 nm)-DPP sample is the only one that overlays with that of the DPP (aggregate)-only sample, while the absorption spectra of the QD (1.6 nm, 2.2 nm, and 2.4 nm)-DPP assemblies are shifted and broadened, we can confirm that these spectral changes are due to co-aggregation of the QDs and DPP.

The transient absorption spectra of DPP-only have three main features (Fig. 3A and B): (i) a relatively broad absorption signal at 460 nm corresponding to the S_1 state formed directly after photoexcitation at 610 nm, which has a lifetime of 13.4 ps; (ii) two narrow absorption bands peaked at 490 and 523 nm that grow in as the S_1 signal decays (with the same rate) corresponding to the T_1 state; and (iii) weak ground state bleach (GSB) signals at 565 and 610 nm, which appear within the IRF of the laser, and undergo a second growth with a time constant of 14 ps. The coordination of the decay of the S_1 (13–14 ps)$^{-1}$ signal with the generation of the T_1 signal and the second growth of the GSB signals unambiguously suggest a singlet fission mechanism, which agrees with previous reports on thin films of DPP.[21] Additionally, the 523 nm peak for T_1 has an additional growth process, with a time constant of 150 ps, after the S_1 signal has decayed completely (the 490 nm T_1 signal overlaps strongly with the S_1 signal such that it is difficult to

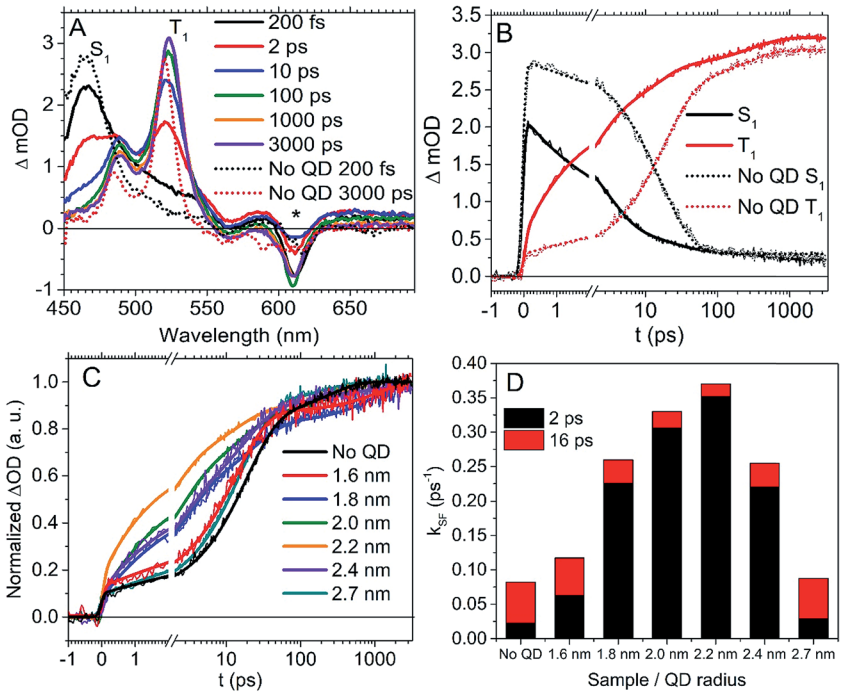

Fig. 3 (A) Selected fs-TA spectra of the QD–DPP ($r = 2.2$ nm) assembly at a series of time delays after excitation at 610 nm showing the decay of S_1 of DPP and the rise of T_1 of DPP. The asterisk indicates the spectral region affected by pump scatter. The dotted lines are the representative spectra of the S_1 and T_1 states of DPP-agg without QDs. (B) The dynamics of SF of DPP with and without QDs. Solid lines: kinetic traces extracted from the TA spectra in (A) at 467 nm (the S_1 absorption of DPP) and 523 nm (the T_1 absorption of DPP), after subtracting the photoinduced absorption (PIA) background from QDs, see the ESI.† Dotted lines: kinetics of DPP aggregates without QDs. The kinetic traces are fit with multi-exponential functions convolved with a Gaussian IRF. (C) Normalized kinetic traces extracted from the TA spectrum of DPP or the QD–DPP assemblies at 523 nm (the T_1 absorption of DPP). The legend indicates the radii of the QDs in the mixtures. The kinetic traces are fit with the convolution of multiple-exponential functions and a Gaussian IRF; two time constants (2 ps and 16 ps) that correspond to the SF process are shared over fits to all kinetic traces and their relative amplitudes are varied. (D) Amplitude-averaged SF rate constants of DPP only and QD–DPP assemblies with various QD radii. The colored segments indicate the relative contributions of 2 ps (black) and 16 ps (red) components of the SF process, obtained from the fits in (C).

track dynamics at 490 nm). Based on previous reports, we assign this rate constant to the dissociation of the triplet pair state, $^1(T_1T_1)$, after the initial singlet fission.[17,26,43–45] The complete SF mechanism can be written as eqn (1),

$$S_1 + S_0 \leftrightarrow {}^{\tau_1=2.7-13.4\ \text{ps}}{}^1(T_1T_1) \overset{\tau_2=150-310\ \text{ps}}{\leftrightarrow} T_1 + T_1 \quad (1)$$

where the rate constants shown are for the range of samples we examined with and without QDs (*vide infra*).

When we pump the QD (2.2 nm)/DPP sample at 610 nm within the TA experiment, both DPP and the PbS QDs are photoexcited. TA spectra at a series of

delay times after photoexcitation are shown in Fig. 3A. Within the spectral region between 480 and 700 nm, PbS QDs have a broad, featureless TA background underneath the DPP signals. A bleach signal caused by the depletion of a higher exciton state appears between 470 and 450 nm, and overlaps with the S_1 signal of DPP (see the ESI†). By comparing the TA spectra of the mixtures with the TA spectra of DPP-only, we determined that, at wavelengths >640 nm, the spectrum only has contributions from the photo-induced absorption (PIA) of PbS QDs. Furthermore, when we excite the mixture at 970 nm, where only PbS QDs absorb, the dynamics of the PIA are the same as if we excited the sample at 610 nm. We can therefore remove the QD PIA background from the raw spectra of QD/DPP by subtracting off from these spectra the spectra collected on the same sample with 970 nm excitation, after appropriately scaling the PIA signals of QDs. A pair of isolated kinetic traces of the S_1 and T_1 states of DPP with QDs ($r = 2.2$ nm) obtained with this procedure are plotted in Fig. 3B (see the ESI† for details). We note that, with DPP present, the PIA signal of PbS QDs ($r = 2.2$ nm) decays with time-constants of 11 and 120 ps, primarily due to hole transfer from the valence band of PbS to DPP. Hole transfer from PbS QDs to pentacene derivatives has been reported previously.[32,46]

We did not observe either triplet-to-triplet energy transfer from QDs to DPP, or the formation of the triplet exciton of DPP following the hole transfer, when PbS QDs were excited within the co-aggregates. These processes are either too slow and therefore outside the temporal window of our TA experiment,[46] or require specific surface sites associated with ligand binding to occur, as suggested by Roberts and coauthors.[47] We also did not observe electron transfer from either the S_1 or T_1 states of DPP to the QDs. It is likely that the fast SF process out-competes electron transfer from S_1, as previously observed for gold nanoparticles,[20] and that the T_1 state of DPP does not have enough energy to donate an electron to the conduction band of the QDs.

Fig. 3A shows the TA spectrum of the QD–DPP ($r = 2.2$ nm) co-aggregate at a series of delay times after pumping at 610 nm. Fig. 3B shows kinetic traces extracted from this spectrum at the peak of the S_1 and T_1 features of DPP. The spectra and kinetics for the QD–DPP samples with QD of all other radii are in the ESI.† The S_1 TA feature of DPP is broader and undergoes a significantly faster decay when 2.2 nm QDs are present than in DPP-only samples (Fig. 3A and B). The growth of the T_1 signals accelerates commensurately. We globally fit the two kinetic traces in Fig. 3B by sharing two time constants between the two fits, allowing the amplitudes to float. We obtain $\tau_1 = 1.8$ ps, and $\tau_2 = 14$ ps. 57% of the amplitude of the triplet signal grows with the time constant τ_1, which corresponds to accelerated SF due to the formation of DPP/QD assemblies. Based on comparison with the DPP-only dynamics, τ_2 corresponds to the SF process in undisturbed DPP-agg (where the molecules are still perpendicularly aligned). The presence of two different SF rates within the same sample of DPP-aggregates implies at least two types of SF sites or local environments, which has been reported in rubrene assemblies.[15,19] A third kinetic component with $\tau_3 = 310$ ps is needed to fit the slow growth of the T_1 signal, and corresponds to the dissociation of T_1 excitons from the triplet pair state, $^1(T_1T_1)$.

Fig. 3C shows that the radius of the QDs influences the degree to which SF is accelerated within the DPP aggregates. We determine the relationship between the size of the QD and the rate of SF by fixing the two fastest time constants for

growth of the T_1 signal to 2 ps and 16 ps (allowing their relative amplitudes to float), and using those two time constants to globally fit the T_1 kinetic traces for all samples. Fig. 3D shows the amplitude-averaged SF rate constants (also listed in Table 1) for samples made with each of six QD sizes, and the breakdown (with respect to amplitude) of the average rate constants into the two fixed components. The most prominent acceleration of SF occurs in the co-aggregates formed with $r = 2.2$ nm QDs, for which the overall averaged SF rate is 5-fold faster than that in DPP-only aggregates. The smallest ($r = 1.6$ nm) and largest QDs (2.7 nm) only marginally increase the rate of SF.

The comparison of ground state absorption, TEM and TA data indicates that the acceleration of SF in DPP is related to the formation of DPP/QD co-aggregates and subsequent disturbance of the perpendicular packing of DPP molecules. The undisturbed DPP crystal structure enables minimal intermolecular coupling between the SF precursor and the S_1 excited state.[21] Any displacement of DPP molecules from this perpendicular alignment will yield a more favorable overlap between HOMO and LUMO among different DPP molecules, and thereby accelerate SF.[2,25,48]

We believe the SF behavior of DPP is not strongly affected by the largest QDs because, for large PbS QDs, the dominant facet of the nanocrystal is (100), which has a low density of surface ligands and therefore a low affinity for DPP.[49] We used quantitative NMR to confirm that, indeed, the 2.7 nm QDs have the smallest average coverage of PEGT (see Table 1 and the ESI†). However, affinity for DPP cannot be the only factor in the size-dependence of this effect because (i) the smallest QDs ($r = 1.6$ nm) with the highest surface ligand density (3.6 nm^{-2}) also form co-aggregates with DPP with minimal effect on SF; and (ii) according to the ground state absorption spectra, the strength of the intermolecular coupling within the co-aggregates of DPP and QDs with $r \leq 2.2$ nm is nearly constant, but the SF rates vary by a factor of three for this set of samples.

We therefore propose that the QDs' ability to modulate the rate of SF also depends on the dielectric environment at the surface of the QD. It is known that the rate of SF, which can be regarded as a double electron transfer process, is accelerated in a more polar environment where charge-separated intermediates are stabilized.[28,29] For the smallest QDs, the predominant (111) facets densely covered with surface ligands (Table 1) favor the formation of co-aggregates, but also surround the DPP with PEG, which has a low dielectric constant ($\varepsilon = \sim 10$) compared to water ($\varepsilon = 80.4$). The effect on SF from the enhancement of intermolecular coupling is therefore counteracted by the decrease in local dielectric constant. Additional evidence that as the QDs get smaller, the DPP is increasingly separated from the QD by PEG is in the comparison of hole transfer rates from the QD to DPP. The rate of this charge transfer process strongly depends on the distance between the DPP and the surface of the QDs. The smallest ($r = 1.6$ nm)

Table 1 NMR-measured surface density of PEGT on PbS QDs of different sizes, and corresponding SF rates within QD–DPP co-aggregates

QD radius (nm)	2.7	2.4	2.2	2.0	1.8	1.6
Density (PEG per nm^2)	1.9	2.2	2.5	2.9	3.3	3.6
SF rates (ps^{-1})	0.088	0.25	0.37	0.33	0.26	0.12

QDs have a slower rate of hole transfer than the $r = 2.2$ nm QDs, despite a greater driving force for the process (see the ESI†). This result implies that DPP is closer and more electronically coupled to the 2.2 nm QD than to the 1.6 nm QD. PbS has a significantly higher dielectric constant ($\varepsilon = 169$) than water and can better stabilize the charge transfer-like SF precursor. We therefore believe that the 2.2 nm QDs have the optimal surface density of PEG to have sufficient affinity for DPP to disturb its aggregate structure, and a high enough local dielectric constant to stabilize the SF precursor. These two factors contribute to a factor-of-five increase in the rate of SF.

The local electric field of the photoinduced charge separated state, $QD^{\bullet -}|DPP^{+}$, formed by hole transfer, could, in principle, affect the SF rate by stabilizing the SF intermediate. We do not believe this effect is significant because: (i) this type of influence would only occur when a $QD^{\bullet -}|DPP^{+}$ state appears close to the SF site, which is very low probability considering our low photon flux (corresponding to <15% of PbS QDs photoexcited per pulse); (ii) the hole transfer process observed in QD/DPP co-aggregates is on a similar or slower time scale (11 and 120 ps) than SF; and (3) charge-separated states would also accelerate the decay of proximate triplet excitons in DPP (a known problem for photovoltaic devices trying to harness SF). We do not however observe faster decay of the T_1 state of DPP within DPP/QD co-aggregates than with DPP only.

Conclusions

We demonstrate systematic control of the SF rate within DPP aggregates by adsorbing those aggregates on PbS QDs of different sizes. The rate of SF can be accelerated by a factor of five using QDs with the optimal size, $r = 2.2$ nm. The acceleration of SF in DPP-agg can be attributed to two factors: (i) the disturbance of the perpendicular molecular packing of DPP, which enhances the intermolecular coupling; and (ii) the high local dielectric environment provided by PbS, which stabilizes the SF precursor. Our work suggests that careful and systematic manipulation of the QD surface environment can affect the excitonic behaviour of the aggregates of adsorbed organic molecules. This work informs strategies for designing SF-promoted photovoltaic and optoelectronic devices based on PbS (or other types of) QDs and polyacene derivatives.

Conflicts of interest

There are no conflicts to declare.

Acknowledgements

This material is primarily based upon work supported by the Air Force Office of Scientific Research, under AFOSR award No. FA-9550-17-1-0271 (synthesis of QD–DPP complexes, stead-state and time-resolved optical measurements), as part of the Center for Bio-Inspired Energy Science, an Energy Frontier Research Center funded by the U.S. Department of Energy (DOE), Office of Science, Basic Energy Sciences (BES), under Award # DE-SC0000989 (TEM measurements), and by the National Science Foundation under Award # CHE-1664184 (NMR measurements).

References

1 M. C. Hanna and A. J. Nozik, *J. Appl. Phys.*, 2006, **100**(7), 0745101–0745108.
2 M. B. Smith and J. Michl, *Chem. Rev.*, 2010, **110**(11), 6891–6936.
3 M. J. Y. Tayebjee, A. A. Gray-Weale and T. W. Schmidt, *J. Phys. Chem. Lett.*, 2012, **3**(19), 2749–2754.
4 C. A. Nelson, N. R. Monahan and X. Y. Zhu, *Energy Environ. Sci.*, 2013, **6**(12), 3508–3519.
5 E. C. Greyson, B. R. Stepp, X. Chen, A. F. Schwerin, I. Paci, M. B. Smith, A. Akdag, J. C. Johnson, A. J. Nozik, J. Michl and M. A. Ratner, *J. Phys. Chem. B*, 2009, **114**(45), 14223–14232.
6 I. Paci, J. C. Johnson, X. D. Chen, G. Rana, D. Popovic, D. E. David, A. J. Nozik, M. A. Ratner and J. Michl, *J. Am. Chem. Soc.*, 2006, **128**(51), 16546–16553.
7 P. M. Zimmerman, Z. Zhiyong and C. B. Musgrave, *Nat. Chem.*, 2010, **2**(8), 24–28.
8 W. L. Chan, M. Ligges, A. Jailaubekov, L. Kaake, L. Miaja-Avila and X. Y. Zhu, *Science*, 2011, **334**(6062), 1541–1545.
9 M. W. B. Wilson, A. Rao, J. Clark, R. S. S. Kumar, D. Brida, G. Cerullo and R. H. Friend, *J. Am. Chem. Soc.*, 2011, **133**(31), 11830–11833.
10 P. M. Zimmerman, F. Bell, D. Casanova and M. Head-Gordon, *J. Am. Chem. Soc.*, 2011, **133**(49), 19944–19952.
11 J. J. Burdett and C. J. Bardeen, *J. Am. Chem. Soc.*, 2012, **134**(20), 8597–8607.
12 N. R. Monahan, D. Sun, H. Tamura, K. W. Williams, B. Xu, Y. Zhong, B. Kumar, C. Nuckolls, A. R. Harutyunyan, G. Chen, H.-L. Dai, D. Beljonne, Y. Rao and X. Y. Zhu, *Nat. Chem.*, 2016, **9**, 341.
13 L. Ma, K. K. Zhang, C. Kloc, H. D. Sun, M. E. Michel-Beyerle and G. G. Gurzadyan, *Phys. Chem. Chem. Phys.*, 2013, **14**(23), 8307–8312.
14 J. J. Burdett and C. J. Bardeen, *Acc. Chem. Res.*, 2013, **46**(6), 1312–1320.
15 S. T. Roberts, R. E. McAnally, J. N. Mastron, D. H. Webber, M. T. Whited, R. L. Brutchey, M. E. Thompson and S. E. Bradforth, *J. Am. Chem. Soc.*, 2012, **134**(14), 6388–6400.
16 A. A. Bakulin, S. E. Morgan, T. B. Kehoe, M. W. B. Wilson, A. W. Chin, D. Zigmantas, D. Egorova and A. Rao, *Nat. Chem.*, 2016, **8**(1), 16–23.
17 B. S. Basel, J. Zirzlmeier, C. Hetzer, B. T. Phelan, M. D. Krzyaniak, S. R. Reddy, P. B. Coto, N. E. Horwitz, R. M. Young, F. J. White, F. Hampel, T. Clark, M. Thoss, R. R. Tykwinski, M. R. Wasielewski and D. M. Guldi, *Nat. Commun.*, 2017, **8**, 15171.
18 A. J. Musser, M. Liebel, C. Schnedermann, T. Wende, T. B. Kehoe, A. Rao and P. Kukura, *Nat. Phys.*, 2015, **11**(4), 352–357.
19 J. N. Mastron, S. T. Roberts, R. E. McAnally, M. E. Thompson and S. E. Bradforth, *J. Phys. Chem. B*, 2013, **117**(49), 15519–15526.
20 D. Kato, H. Sakai, N. V. Tkachenko and T. Hasobe, *Angew. Chem.*, 2016, **128**(17), 5316–5320.
21 S. R. Yost, J. Lee, M. W. B. Wilson, T. Wu, D. P. McMahon, R. R. Parkhurst, N. J. Thompson, D. N. Congreve, A. Rao, K. Johnson, M. Y. Sfeir, M. G. Bawendi, T. M. Swager, R. H. Friend, M. A. Baldo and T. Van Voorhis, *Nat. Chem.*, 2014, **6**(6), 492–497.

22 C. Ramanan, A. L. Smeigh, J. E. Anthony, T. J. Marks and M. R. Wasielewski, *J. Am. Chem. Soc.*, 2012, **134**(1), 386–397.
23 E. C. Greyson, J. Vura-Weis, J. Michl and M. A. Ratner, *J. Phys. Chem. B*, 2010, **114**(45), 14168–14177.
24 C. Wang, M. Angelella, C. H. Kuo and M. J. Tauber, *Proc. SPIE: Phys. Chem. Interf. Nanomater.*, vol. XI, 2012, pp. 8459051–8459113.
25 R. D. Pensack, A. Tilley, C. Grieco, G. Purdum, E. Ostroumov, D. B. Granger, D. Oblinksy, J. Dean, G. Doucette, J. Asbury, Y.-L. Loo, D. Seferos, J. E. Anthony and G. Scholes, *Chem. Sci.*, 2018, **9**(29), 6240–6259.
26 R. D. Pensack, C. Grieco, G. E. Purdum, S. M. Mazza, A. J. Tilley, E. E. Ostroumov, D. S. Seferos, Y.-L. Loo, J. B. Asbury, J. E. Anthony and G. D. Scholes, *Mater. Horiz.*, 2017, **4**(5), 915–923.
27 C. M. Mauck, P. E. Hartnett, Y. L. Wu, C. E. Miller, T. J. Marks and M. R. Wasielewski, *Chem. Mater.*, 2017, **29**(16), 6810–6817.
28 S. Hart, W. R. Silva and R. R. Frontiera, *Chem. Sci.*, 2018, **9**(5), 1242–1250.
29 B. S. Basel, J. Zirzlmeier, C. Hetzer, S. R. Reddy, B. T. Phelan, M. D. Krzyaniak, M. K. Volland, P. B. Coto, R. M. Young, T. Clark, M. Thoss, R. R. Tykwinski, M. R. Wasielewski and D. M. Guldi, *Chem*, 2018, **4**(5), 1092–1111.
30 N. J. Thompson, M. W. B. Wilson, D. N. Congreve, P. R. Brown, J. M. Scherer, T. S. Bischof, M. Wu, N. Geva, M. Welborn, T. V. Voorhis, V. Bulović, M. G. Bawendi and M. A. Baldo, *Nat. Mater.*, 2014, **13**(11), 1039–1043.
31 M. Tabachnyk, B. Ehrler, S. Gélinas, M. L. Böhm, B. J. Walker, K. P. Musselman, N. C. Greenham, R. H. Friend and A. Rao, *Nat. Mater.*, 2014, **13**(11), 1033–1038.
32 B. Ehrler, M. W. B. Wilson, A. Rao, R. H. Friend and N. C. Greenham, *Nano Lett.*, 2012, **12**(2), 1053–1057.
33 P. J. Jadhav, P. R. Brown, N. Thompson, B. Wunsch, A. Mohanty, S. R. Yost, E. Hontz, T. Van Voorhis, M. G. Bawendi, V. Bulovic and M. A. Baldo, *Adv. Mater.*, 2012, **24**(46), 6169–6174.
34 B. J. Walker, G. P. Nair, L. F. Marshall, V. Bulović and M. G. Bawendi, *J. Am. Chem. Soc.*, 2009, **131**(28), 9624–9625.
35 J. E. Halpert, J. R. Tischler, G. Nair, B. J. Walker, W. Liu, V. Bulovic and M. G. Bawendi, *J. Phys. Chem. A*, 2009, **113**(23), 9986–9992.
36 E. A. McArthur, J. M. Godbe, D. B. Tice and E. A. Weiss, *J. Phys. Chem. A*, 2012, **116**(10), 6136–6142.
37 C. Wang and E. A. Weiss, *J. Am. Chem. Soc.*, 2016, **138**(30), 9557–9564.
38 D. Savateeva, D. Melnikau, V. Lesnyak, N. Gaponik and Y. P. Rakovich, *J. Mater. Chem.*, 2012, **22**(21), 10816–10820.
39 M. A. Hines and G. D. Scholes, *Adv. Mater.*, 2003, **15**(21), 1844–1849.
40 E. A. McArthur, A. J. Morris-Cohen, K. E. Knowles and E. A. Weiss, *J. Phys. Chem. B*, 2010, **114**(45), 14514–14520.
41 F. C. Spano, *Acc. Chem. Res.*, 2010, **43**(3), 429–439.
42 J. Knoester and F. C. Spano, *Theory of pump-probe spectroscopy of molecular J-aggregates*, in Host Publication, World Scientific Publishing, 1996, pp. 111–160.
43 R. D. Pensack, E. E. Ostroumov, A. J. Tilley, S. Mazza, C. Grieco, K. J. Thorley, J. B. Asbury, D. S. Seferos, J. E. Anthony and G. D. Scholes, *J. Phys. Chem. Lett.*, 2016, **7**(13), 2370–2375.

44 R. D. Pensack, A. J. Tilley, S. R. Parkin, T. S. Lee, M. M. Payne, D. Gao, A. A. Jahnke, D. G. Oblinsky, P.-F. Li, J. E. Anthony, D. S. Seferos and G. D. Scholes, *J. Am. Chem. Soc.*, 2015, **137**(21), 6790–6803.
45 B. D. Folie, J. B. Haber, S. Refaely-Abramson, J. B. Neaton and N. S. Ginsberg, *J. Am. Chem. Soc.*, 2018, **140**(6), 2326–2335.
46 S. Garakyaraghi, C. Mongin, D. B. Granger, J. E. Anthony and F. N. Castellano, *J. Phys. Chem. Lett.*, 2017, 1458–1463.
47 J. A. Bender, E. K. Raulerson, X. Li, T. Goldzak, P. Xia, T. Van Voorhis, M. L. Tang and S. T. Roberts, *J. Am. Chem. Soc.*, 2018, **140**(24), 7543–7553.
48 M. J. Y. Tayebjee, K. N. Schwarz, R. W. MacQueen, M. Dvořák, A. W. C. Lam, K. P. Ghiggino, D. R. McCamey, T. W. Schmidt and G. J. Conibeer, *J. Phys. Chem. A*, 2016, **120**(1), 157–165.
49 H. Choi, J.-H. Ko, Y.-H. Kim and S. Jeong, *J. Am. Chem. Soc.*, 2013, **135**(14), 5278–5281.